RSC Advances

PAPER

View Article Online
View Journal | View Issue

Cite this: *RSC Adv.*, 2017, **7**, 37194

Trace-doped metal–organic gels with remarkably enhanced luminescence†

Xiying Feng, Lihua Zeng, Dianting Zou, Zizhe Zhang, Guihao Zhong, Shuyin Peng, Liping Liu, Liuping Chen and Jianyong Zhang *

Received 23rd May 2017
Accepted 20th July 2017

DOI: 10.1039/c7ra05783k

rsc.li/rsc-advances

A novel approach has been proposed to fabricate MOF-based luminescent gel materials with trace amounts of doping in order to study the role of trace defects in metal–organic gel materials. UiO-66-based ZrBDC (BDC = 1,4-benzene dicarboxylate) gels were first prepared from Zr^{4+} and H_2BDC under mild conditions, and subsequently trace doping (as low as 0.01 mol%) of the ZrBDC gel materials with H_4TCPE (tetrakis(4-carboxyphenyl)ethylene) was achieved successfully. The resulting **ZrBDC–TCPE0.01%** gel material features mild synthetic conditions and retains the high porosity of parent UiO-66 gel materials. Moreover, trace doping causes a remarkable change to the luminescence properties and the gel emits blue luminescence with high quantum yield (59%). **ZrBDC–TCPE0.01%** shows responses with high sensitivity and selectivity for nitroaromatics (picric acid) in the aqueous phase and detects picric acid as low as parts per billion (24 ppb). The present luminescent gel materials provide new insights into developing functional metal–organic materials through trace defects, which may remarkably alter the properties of metal–organic materials.

Introduction

Defected materials can give rise to a large range of optical, electronic, magnetic, conductive and other physical properties. The materials properties can be tuned and optimized by controlling the defect composition. For example, in traditional inorganic luminescent materials, doping other elements into the main body is classic approach to tune the emissive performance. As a catalogue of porous materials, metal–organic frameworks (MOFs) from the self-assembly of inorganic and organic building blocks usually form highly ordered crystalline solids, and discussions about the properties of MOFs focus mainly on features revealed by the crystal structures. However, the crystal structures of MOFs may not fully relate to their physical properties, and defects or deviations from an ideally ordered crystal structure have been recently shown to significantly affect their properties.[1–6] There are several methods to create defects in MOFs, including doping with another ligand or metal element into the linkers or the inorganic nodes, missing linkers or components, and partial ligand replacement or metal ion replacement.[7–16] Among these methods doping has been shown to produce novel properties while maintaining the parent framework topologies,[7–14,17] thus providing abundant opportunities in catalysis, sorption, magnetic, optical, conductive materials, and so on. However, all these studies focus on stoichiometric loading of defects (typically >10 mol%) and the role of trace defects has been given little regard.

In the present work we propose a novel approach for fabricating MOF-based gel materials with trace-doped-enhancement luminescence. MOF-based gel materials are assembled from MOF nanoparticles, combining the advantages of MOFs and of gels.[18–22] UiO-66-based ZrBDC (BDC = 1,4-benzene dicarboxylate) gel materials have been developed as new members of these materials. Subsequent trace doping (as low as 0.01 mol%) of the gel materials with tetraphenylethylene (TPE) lumiphore has been achieved (Fig. 1). The resulting materials have three features. (1) MOFs offer a platform with high surface areas, tuneable framework composition. Among them, UiO-66-type MOFs have Zr_6-based robust and porous networks with high connectivity with each $[Zr_6(\mu_3\text{-}O)_4(\mu_3\text{-}OH)_4]^{12+}$ node linked to 12 carboxylates of 1,4-benzene dicarboxylate ligands,[23–25] showing high thermal and chemical stability.[26–29] (2) Gelation is a powerful method to prepare micro-meso-macroporous hierarchical metal–organic materials with surface and inherent defects under mild conditions.[30–34] It may scale down MOF crystallites to the nanosize regime and implement hierarchical porosity to overcome diffusion limitations.[18–22] (3) Materials with trace doping may be interesting because it may save expensive luminescent materials and avoid some problems caused by high doping concentration such as unstable luminescence and device aging. Additionally trace-doped materials are generally isostructural to the parent ones, thus it is easy to

Sun Yat-Sen University, Lehn Institute of Functional Materials, MOE Laboratory of Bioinorganic and Synthetic Chemistry, Guangzhou 510275, China. E-mail: zhjyong@mail.sysu.edu.cn

† Electronic supplementary information (ESI) available: Experimental details, photos, SEM and TEM images, EDX, IR, XPS spectra, TGA and luminescence data. See DOI: 10.1039/c7ra05783k

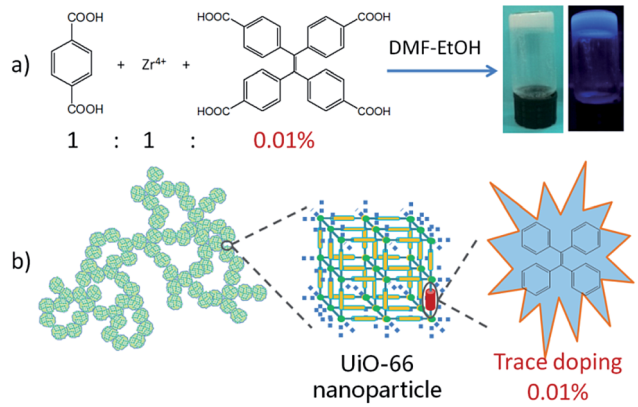

Fig. 1 (a) Preparation of **ZrBDC–TCPE0.01%** gel from 1,4-benzenedicarboxylic acid (H_2BDC), Zr^{4+}, and tetrakis(4-carboxyphenyl) ethylene (H_4TCPE). The photos were taken under day light (left) and under irradiation with 365 nm ultraviolet light (right). The bottles are kept inverted to confirm the gel formation. (b) Schematic illustration for the construction of **ZrBDC–TCPE0.01%** gel.

predict the outcome structure and the synthesis of functionalized materials becomes versatile and applicable.

Results and discussion

First, parent ZrBDC gels were prepared through reaction of 1,4-benzenedicarboxylic acid (H_2BDC) with $ZrCl_4$ in DMF–EtOH (v/v 1 : 1) upon mild heating at 80 °C (Fig. S1 and Table S1†).[20,21] When the molar ratio of Zr/BDC ranges from 1 : 1 to 2 : 1, white opaque gels were obtained within 1–1.5 h. **ZrBDC-1:1-0.15** gel, denoting the molar ratio of Zr/BDC is 1 : 1 and the concentration is 0.15 mol L^{-1} based on BDC, was chosen and investigated in detail. SEM investigations show that the gels have porous networked structures consisting of cross-linked particles, and TEM investigations verify that the agglomerated nanoparticles with 50–100 nm sizes are irregularly interconnected, spanning large void spaces and sustaining the gel matrix (Fig. 2a and b). PXRD was applied to establish the microstructures of the gel materials. The ZrBDC gel materials possess powder X-ray diffraction (PXRD) patterns that are remarkably consistent with that reported for the UiO-66 topology (Fig. 3).[35] This implies that the gels consist of crystalline components of MOF structure, that is, an ordered 3D framework of $Zr_6O_4(OH)_4(BDC)_6$ that are bridged by the 1,4-benzene dicarboxylate linkers. The broadness of the diffraction peaks indicates that the MOF components in the gel are nanoparticles (71 nm for **ZrBDC-1:1-0.15**, as simulated by the Scherer equation), which is in agreement with the SEM and TEM observations. Therefore the present **ZrBDC-1:1-0.15** gel material has a porous networked structure consisting of cross-linked UiO-66 MOF nanoparticles.

To create luminescent gels, tetraphenylethylene (TPE) lumiphore is subsequently introduced into the **ZrBDC-1:1-0.15** gel *via* trace doping of tetrakis(4-carboxyphenyl)ethylene (H_4TCPE). In this strategy TCPE is an inherent component as the organic struts for the construction of the gel matrix *via* coassembly of two ligands into gels. TCPE groups replace part of the 1,4-benzenedicarboxylate linkers in the gel material,

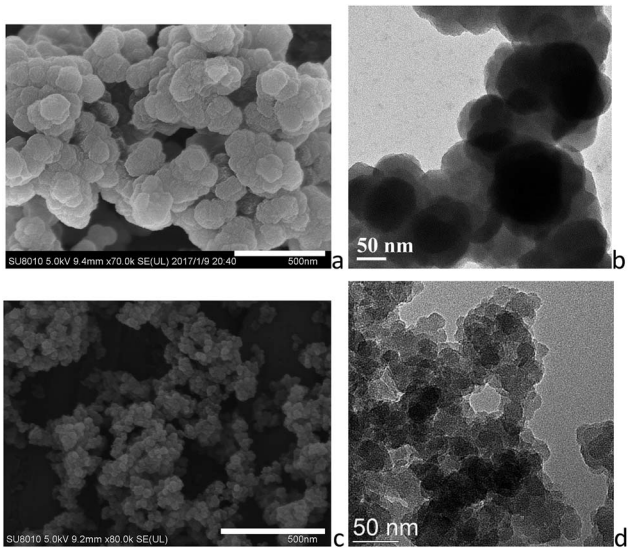

Fig. 2 (a) SEM and (b) TEM images of **ZrBDC-1:1-0.15**, and (c) SEM and (d) TEM images of **ZrBDC–TCPE0.01%**. Scale bars represent 500 nm for SEM images.

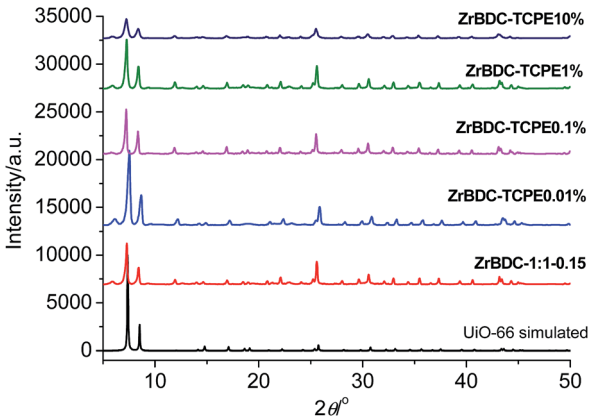

Fig. 3 PXRD patterns of (from bottom to top) simulated UiO-66, **ZrBDC-1:1-0.15**, **ZrBDC–TCPE*x*** (x = 0.01, 0.1, 1, 10%) wet gels. The patterns are vertically offset for clarity.

creating luminescent gel materials. Additionally TPE features aggregation-induced emission (AIE) characteristics showing highly enhanced emission in the aggregate state.[36] Immobilization of H_4TCPE into a rigid framework may inhibit the rotation and torsion of phenyl rings, leading to increased quantum yield.[37–41] **ZrBDC-1:1-0.15** gel with trace doping (0.01%) of TCPE was prepared, synthetically 0.01% equivalent of H_4TCPE with respect of H_2BDC was used to prepare metal–organic gels, and the sample is denoted as **ZrBDC–TCPE0.01%** (Fig. 1). For comparison **ZrBDC–TCPE*x*** (x = 0.1, 1, 10%) gels were also prepared (Fig. S1†). In order to characterize the porosity, the solvent in the wet gels was removed by centrifugation and exchanged with ethanol, and the resulting materials were dried by subcritical CO_2(l) to obtain dried materials as crushed solid.

SEM and TEM reveal that the introducing of TCPE does not affect the morphology significantly, showing similar porous

structures with cross-linked nanoparticles (Fig. 2c, d and S2–S4†). In comparison **ZrBDC–TCPE0.01%** consists of smaller nanoparticles with *ca.* 20–50 nm size. The gels give well-resolved PXRD patterns with salient peaks that precisely match the simulated patterns of single-crystal UiO-66, indicating that the crystallinity of UiO-66 is maintained (Fig. 3). The crystallite size of is *ca.* 41 nm for **ZrBDC–TCPE0.01%**, as simulated by the Scherer equation. The smaller nanoparticles may be attributed to the presence of increasing surface and inherent defects in the trace-doped materials.

ZrBDC–TCPE0.01% gel was also characterized by other analytical techniques including FT-IR, EDX and XPS (Fig. S5–S11†), but no difference could be identified as expected due to the trace presence of TCPE. FT-IR spectra account for the presence of carboxylate in the metal coordination sphere, as evidenced by the C=O asymmetric stretching at around 1580 cm^{-1}. Elemental composition analysis by energy dispersive X-ray spectroscopy (EDX) reveals that trace of Cl was present as well in the gels which originate from the precursors. X-ray photoelectron spectroscopy (XPS) analysis shows that the Zr $3d_{3/2}$ and $3d_{5/2}$ binding energies are 185.2 and 182.8 eV, respectively, confirming the presence of highly oxidized tetravalent zirconium.

Thermogravimetric analysis (TGA) profiles of **ZrBDC-1:1-0.15** and **ZrBDC–TCPE0.01%** exhibit continuous weight loss of 56%, related to the removal of moisture, free solvent and ligand and they may remain thermally stable up to *ca.* 550 °C (Fig. S12†). In the TGA profile of **ZrBDC-1:1-0.15**, a weight loss from 68 wt% to 44 wt% between 500 and 600 °C means that the as-synthesized material is defective, exhibiting about 8 BDC ligands per $Zr_6O_4(OH)_4$ cluster. In the TGA profile of **ZrBDC–TCPE0.01%**, the weight loss from 71 wt% to 46 wt% between 500 and 600 °C is consistent with a BDC : Zr_6 ratio of 8, in line with similar linker deficiency.[42] Such defective UiO-66 materials[43–46] may be produced because the present synthesis temperature was low.[47]

To evaluate the porosity, N_2 adsorption–desorption isotherms were collected for the dried materials (Fig. 4 and Table S2†). For **ZrBDC-1:1-0.15**, the BET surface area is 1140–1236 $m^2\ g^{-1}$ and the total pore volume is 0.929–1.107 $cm^3\ g^{-1}$ (two parallel measurements). Its microporosity nature was indicated by rapid gas sorption at low relative pressure (P/P_0 < 0.05). Pore size distributions obtained by nonlocal density functional theory (NLDFT) show main pore size centred at *ca.* 1.11 and 1.27 nm, interpreted as octahedral cages in the pristine UiO-66 structure as well as defect-related regions.[48] The trace doping with TCPE (0.01%, 0.1%) does not show much effect on the porosity of gel materials. For **ZrBDC–TCPE0.01%**, the BET surface area is 1145–1280 $m^2\ g^{-1}$ and the total pore volume is 0.598–0.832 $cm^3\ g^{-1}$ (two parallel measurements). Additionally the pore size does not change greatly with main pore size centred at *ca.* 1.11 and 1.27 nm. This is consistent with the reported data with only 8 linkers per node[44] and the above TG data. However, the BET surface areas (1044–901 $m^2\ g^{-1}$) and pore volumes (0.613–0.682 $cm^3\ g^{-1}$) decrease with high doping concentration of TCPE (1%, 10%).

The photoluminescence property of **ZrBDC–TCPE*x*** gel materials synthesized with various doping concentration

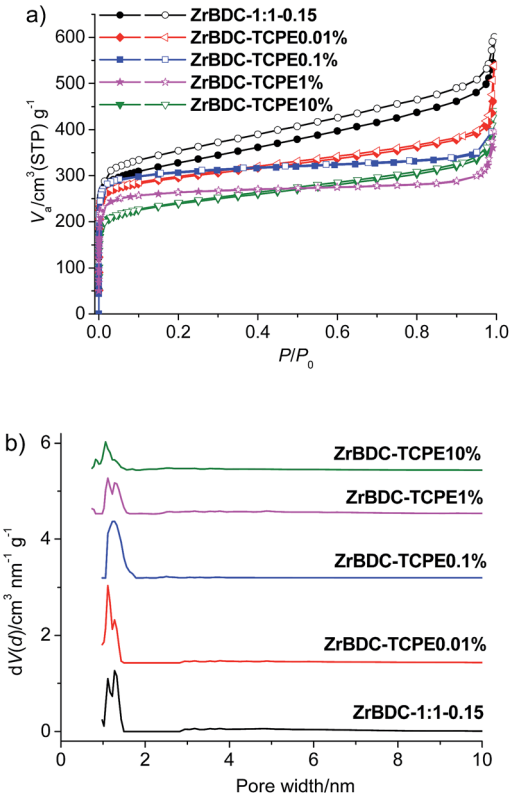

Fig. 4 (a) N_2 adsorption–desorption isotherms (solid symbols represent adsorption, open symbols represent desorption), and (b) NL-DFT pore size distribution (model: N_2 at 77 K on silica (cylinder pore, NLDFT adsorption branch model)) for ZrBDC–TCPE*x* (x = 0.01, 0.1, 1, 10%) and ZrBDC-1:1-0.15. NL-DFT curves are vertically offset for clarity.

(0.01–10% of TCPE with respect to BDC) was examined (Fig. 5a, S13 and Table S3†). **ZrBDC-1:1-0.15** gel is nearly weakly emissive with an emission band at about 498 nm and a fluorescence quantum yield of 14% in gel state. The fluorescence spectra of **ZrBDC–TCPE*x*** gels display an obvious blue shift and the corresponding emission efficiency increases remarkably. In contrast to **ZrBDC-1:1-0.15** gel, **ZrBDC–TCPE0.01%** is highly emissive. The fluorescence is blue-shifted with an emission maximum at 461 nm, which originate from the ligand-based π–π* transition. The fluorescence efficiency of **ZrBDC–TCPE0.01%** is as high as 59%, much higher than that of the parent gel. The time-resolved emission-decay behaviours show that the weighted mean lifetime is 3.32 ns for **ZrBDC–TCPE0.01%**.

The emission peak wavelengths for the **ZrBDC–TCPE*x*** gels dispersed in water range from 461 nm (x = 0.01%) to 521 nm (x = 10%). With increasing content of TCPE, the emission wavelengths presented a red-shift. The emission of the **ZrBDC–TCPE*x*** gels with higher content of TCPE move closer to that of the **ZrTCPE** gel (λ_{em} = 540 nm). Thus the emission of **ZrBDC–TCPE0.01%** mainly ascribe to the homogeneous distribution of TCPE in the framework. The porous network of ZrBDC UiO-66 nanoparticles sterically inhibits the TPE fluorophores from approaching each other and prevents the aggregation of TCPE molecules. This leads to the blue-shifted emission of **ZrBDC–TCPE0.01%** in comparison with **ZrTCPE**. The blue shift in the emission is obvious when the doping concentration is low.

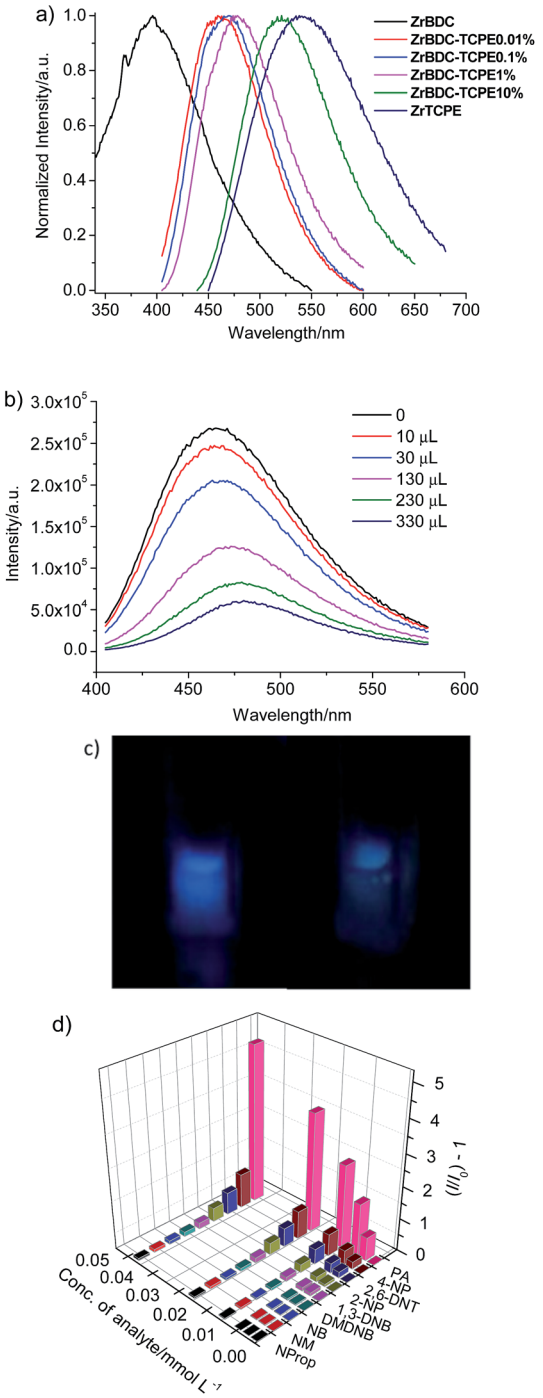

Fig. 5 (a) Normalized emission spectra of **ZrBDC–TCPE*x*** (x = 0.01, 0.1, 1, 10%), **ZrBDC-1:1-0.15**, and **ZrTCPE** gels dispersed in water (10 g L^{-1}). (b) Fluorescence spectra of **ZrBDC–TCPE0.01%** gel dispersed in water (10 g L^{-1}) upon incremental addition of an aqueous solution of PA (0–330 μL, 0.1 mmol L^{-1}) (λ_{ex} = 363 nm). (c) Visual detection of PA (2.3 ppm, 1.0 × 10^{-5} mol L^{-1}) with **ZrBDC–TCPE0.01%** gel dispersed in water (10 g L^{-1}) (right) and blank dispersion (left). The photographs were taken under 365 nm UV irradiation. (d) Stern–Volmer plots of various nitro analytes in water for **ZrBDC–TCPE0.01%**.

The unique porosity and the fluorescence of **ZrBDC–TCPE*x*** gels prompted us to explore their potential application as fluorescent sensors for nitroexplosives. The open framework structure of **ZrBDC–TCPE*x*** gels with high surface area and large pore windows may facilitate guest diffusion across the frameworks and easily interact with active lumiphore sites. Herein picric acid (PA) was used as a model nitroexplosive (Scheme S1†). Fluorescence quenching titrations with various PA concentrations were conducted at room temperature in aqueous solution because aqueous-phase detection is preferred for probing of nitro explosives in soil or groundwater.[49] The gels were readily dispersed in water with a concentration of 10 g L^{-1} for detection. The fluorescent intensity gradually decreases with the addition of PA into **ZrBDC–TCPE0.01%** (Fig. 5b, c and S14†). The Stern–Volmer (SV) equation of the relative fluorescence intensity *vs.* PA concentration in aqueous solution is $I_0/I = K_{SV}[A] + 1$, where I_0 and I are the photoluminescence intensities before and after addition of the analyte, respectively, and [A] is the molar concentration of the analyte. K_{SV} is the quenching constant (L mol^{-1}). The relative fluorescence intensity is linear with the concentration suggesting the quenching is mainly diffusion-limited. The quenching constant for PA is 2.91 × 10^5 L mol^{-1} in the low concentration range (0–0.53 mol L^{-1}) (R^2 = 0.9962), which is remarkably higher than that of a closely related TPE-modified Zr-MOF (2.8 × 10^4 L mol^{-1}),[50] lying amongst the highest of the known luminescent MOF-based sensors.[51–53] The limit of detection (LOD) is calculated by the fluorescence quenching data using the 3σ/slope criteria using the equation LOD = 3σ/m, where σ is the standard deviation of blank measurements, and m is the slope between the fluorescence intensity and analyte concentration. The LOD is 1.05 × 10^{-7} mol L^{-1} (24 ppb) for **ZrBDC–TCPE0.01%**. Interestingly, both the quenching constant and the LOD decrease when the doping concentration of TCPE is higher for the **ZrBDC–TCPE*x*** gels (Fig. S15 and S16†). The quenching constant is 1.82 × 10^5 and 5.64 × 10^4 L mol^{-1} and the LOD is 1.98 × 10^{-7} (45 ppb) and 5.25 × 10^{-7} (120 ppb) for **ZrBDC–TCPE0.1%** and **ZrBDC–TCPE1%**, respectively. Therefore, the present gel material with trace doping of TCPE greatly enhances fluorescence response efficiency and demonstrates the potential as a novel type of highly sensitive sensors for PA in aqueous phase.

Fluorescence quenching titrations were also performed with nitroaromatic compounds with similar chemical structures such as 2,6-dinitrophenol (2,6-DNP), 1,3-dinitrobenzene (1,3-DNB), 4-nitrophenol (4-NP), 2-nitrophenol (2-NP) and nitrobenzene (NB), and nitro-aliphatic compounds such as 2,3-dimethyl-2,3-dinitrobutane (DMDNB), 1-nitropropane (NProp) and nitromethane (NM) (Scheme S1†). In a typically designed experimental protocol, the fluorescence spectrum for **ZrBDC–TCPE0.01%** dispersed in water was monitored upon the incremental addition of an aqueous solution of nitroaromatic compounds. Different extents of fluorescence quenching take place upon the addition of the same amount of various analytes (400 μL of 0.1 mM) (Fig. 5d and S17–S25†). The fluorescence quenching efficiencies of various analytes are calculated using the equation $(I_0 - I)/I_0 \times 100\%$, where I_0 and I are the fluorescence intensities of **ZrBDC–TCPE0.01%** before and after the addition of the analytes. The fluorescence quenching efficiencies are in the order, PA (83.1%) ≫ 4-NP (51.8%) > 2,6-DNT (41.2%) > 2-NP (30.0%) > 1,3-DNB (15.6%) >

DMDNB (12.3%) > NB (10.0%) > NM (8.6%) > 1-NProp (6.6%). It suggests that PA shows significant and sensitive fluorescence quenching, while other nitroaromatic compounds with similar chemical structures have much lower fluorescence quenching efficiencies.

The quenching mechanism may be proposed as follow. The tested analytes have suitable sizes (*e.g.*, PA 5.0 × 6.2 × 7.1 Å) to enter the pores of gel nanoparticles.[54] The selective fluorescence quenching for PA may be attributed to energy transfer of the excited-state electron of **ZrBDC–TCPE0.01%** to the electron-deficient PA molecule with its electron-withdrawing $-NO_2$ group. The absorption bands of the analyte PA display considerable overlap with the emission spectra of **ZrBDC–TCPE0.01%**, while nearly absent overlap in the cases of other nitro compounds (Fig. S26†). Resonance energy transfer can effectively occur from the fluorophore to non-emitting analytes. In addition, the fluorescence emission decays instantly upon the addition of PA solution into **ZrBDC–TCPE1%** and maintain an equilibration afterwards (Fig. S26†). The decay time is short to fall in the data collection time of the fluorometer (<1 min). It suggests facile diffusion (mass transfer) of PA across the porous gel network of **ZrBDC–TCPE0.01%**.

Conclusions

In summary, we develop a facile and simple gelation approach for fabricating highly luminescent UiO-66 MOF based ZrBDC materials with trace doping of TPE lumiphor (as low as 0.01%). TCPE groups replace part of the BDC linkers in the parent gel material and the TPE chromophore is incorporated dilutely into the UiO-66 MOF nanoparticle matrix, creating highly luminescent materials. The gel material **ZrBDC–TCPE0.01%** displays the merits of MOFs, gels and trace doping. It consists of interconnected highly porous MOF nanoparticles having the framework structure of UiO-66 and the unique feature of trace occupied TCPE sites (0.01%), causing large change to its luminescent properties. The aqueous dispersion of **ZrBDC–TCPE0.01%** gel emits blue luminescence with high quantum yield. It shows ability to selectively identify the presence of a trace quantity of nitroaromatic explosive in aqueous phase through fluorescence quenching, attractive in virtue of high sensitivity, and rapid response time. These results demonstrate that trace defective sites within metal–organic materials can significantly alter the properties, showing that this class of gel materials and MOFs can serve as a tunable porous platform for novel applications. The method may be utilized for the design of functional porous materials which incorporate a fraction of functional sites into a known phase built from simpler building blocks to avoid tedious synthesis.

Acknowledgements

We gratefully acknowledge the NSFC (51573216), the NSF of Guangdong Province (S2013030013474) and the FRF for the Central Universities (16lgjc66) for financial support.

Notes and references

1 T. D. Bennett, A. K. Cheetham, A. H. Fuchs and F.-X. Coudert, *Nat. Chem.*, 2017, **9**, 11–16.
2 Z. Fang, B. Bueken, D. E. De Vos and R. A. Fischer, *Angew. Chem., Int. Ed.*, 2015, **54**, 7234–7254.
3 H. Furukawa, U. Müller and O. M. Yaghi, *Angew. Chem., Int. Ed.*, 2015, **54**, 3417–3430.
4 D. S. Sholl and R. P. Lively, *J. Phys. Chem. Lett.*, 2015, **6**, 3437–3444.
5 A. Dhakshinamoorthy, A. M. Asiri and H. Garcia, *Catal. Sci. Technol.*, 2016, **6**, 5238–5261.
6 J. Canivet, M. Vandichel and D. Farrusseng, *Dalton Trans.*, 2016, **45**, 4090–4099.
7 S. S. Han and W. A. Goddard III, *J. Am. Chem. Soc.*, 2007, **129**, 8422–8423.
8 Y. Cui, H. Xu, Y. Yue, Z. Guo, J. Yu, Z. Chen, J. Gao, Y. Yang, G. Qian and B. Chen, *J. Am. Chem. Soc.*, 2012, **134**, 3979–3982.
9 X. Zhang, B. Li, H. Ma, L. Zhang and H. Zhao, *ACS Appl. Mater. Interfaces*, 2016, **8**, 17389–17394.
10 R.-Y. Chen, D. Tian, Y.-W. Li, Y.-B. Lv, H.-W. Sun, Z. Chang and X.-H. Bu, *RSC Adv.*, 2015, **5**, 24655–24660.
11 F. Vermoortele, B. Bueken, G. Le Bars, B. V. de Voorde, M. Vandichel, K. Houthoofd, A. Vimont, M. Daturi, M. Waroquier, V. Van Spey-broeck, C. Kirschhock and D. E. De Vos, *J. Am. Chem. Soc.*, 2013, **135**, 11465–11468.
12 C. Wang, Z. Xie, K. E. deKrafft and W. Lin, *J. Am. Chem. Soc.*, 2011, **133**, 13445–13454.
13 C. Wang, D. Liu, Z. Xie and W. Lin, *Inorg. Chem.*, 2014, **53**, 1331–1338.
14 S. Marx, W. Kleist and A. Baiker, *J. Catal.*, 2011, **281**, 76–87.
15 Z. Fang, J. P. Dürholt, M. Kauer, W. Zhang, C. Lochenie, B. Jee, B. Albada, N. Metzler-Nolte, A. Pöppl, B. Weber, M. Muhler, Y. Wang, R. Schmid and R. A. Fischer, *J. Am. Chem. Soc.*, 2014, **136**, 9627–9636.
16 J. Park, Z. U. Wang, L.-B. Sun, Y.-P. Chen and H.-C. Zhou, *J. Am. Chem. Soc.*, 2012, **134**, 20110–20116.
17 P. Falcaro and S. Furukawa, *Angew. Chem., Int. Ed.*, 2012, **51**, 8431–8433.
18 A. K. Chaudhari, I. Han and J.-C. Tan, *Adv. Mater.*, 2015, **27**, 4438–4446.
19 J. J. Marrero-Telladoa and D. D. Díaz, *CrystEngComm*, 2015, **17**, 7978–7985.
20 L. Li, S. Xiang, S. Cao, J. Zhang, G. Ouyang, L. Chen and C. Y. Su, *Nat. Commun.*, 2013, **4**, 1774–1782.
21 L. Liu, J. Zhang, H. Fang, L. Chen and C.-Y. Su, *Chem.–Asian J.*, 2016, **11**, 2278–2283.
22 Q. Wei and S. L. James, *Chem. Commun.*, 2005, 1555–1556.
23 J. H. Cavka, S. Jakobsen, U. Olsbye, N. Guillou, C. Lamberti, S. Bordiga and K. P. Lillerud, *J. Am. Chem. Soc.*, 2008, **130**, 13850–13851.
24 J. B. DeCoste, G. W. Peterson, B. J. Schindler, K. L. Killops, M. A. Broweb and J. J. Mahle, *J. Mater. Chem. A*, 2013, **1**, 11922–11932.
25 M. Kandiah, M. H. Nilsen, S. Usseglio, S. Jakobsen, U. Olsbye, M. Tilset, C. Larabi, E. A. Quadrelli, F. Bonino and K. P. Lillerud, *Chem. Mater.*, 2010, **22**, 6632–6640.

26 G. E. Cmarik, M. Kim, S. M. Cohen and K. S. Walton, *Langmuir*, 2012, **28**, 15606–15613.
27 M. J. Katz, S.-Y. Moon, J. E. Mondloch, M. H. Beyzavi, C. J. Stephenson, J. T. Hupp and O. K. Farha, *Chem. Sci.*, 2015, **6**, 2286–2291.
28 D. Yang, S. O. Odoh, T. C. Wang, O. K. Farha, J. T. Hupp, C. J. Cramer, L. Gagliardi and B. C. Gates, *J. Am. Chem. Soc.*, 2015, **137**, 7391–7396.
29 H. G. T. Nguyen, N. M. Schweitzer, C.-Y. Chang, T. L. Drake, M. C. So, P. C. Stair, O. K. Farha, J. T. Hupp and S. T. Nguyen, *ACS Catal.*, 2014, **4**, 2496–2500.
30 P. Dastidar, S. Ganguly and K. Sarkar, *Chem.–Asian J.*, 2016, **11**, 2484–2498.
31 M.-O. M. Piepenbrock, G. O. Lloyd, N. Clarke and J. W. Steed, *Chem. Rev.*, 2010, **110**, 1960–2004.
32 D. Vallejo-Sánchez, P. Amo-Ochoa, G. Beobide, O. Castillo, M. Fröba, F. Hoffmann, A. Luque, P. Ocón and S. Pérez-Yáñez, *Adv. Funct. Mater.*, 2017, 1605448.
33 A. Mahmood, W. Xia, N. Mahmood, Q. Wang and R. Zou, *Sci. Rep.*, 2015, **5**, 10556.
34 P. Sutar and T. K. Maji, *Chem. Commun.*, 2016, **52**, 8055–8074.
35 S. J. Garibay and S. M. Cohen, *Chem. Commun.*, 2010, **46**, 7700–7702.
36 Y. Dong, J. W. Y. Lam, A. Qin, J. Liu, Z. Li and B. Z. Tang, *Appl. Phys. Lett.*, 2007, **91**, 011111.
37 N. B. Shustova, B. D. McCarthy and M. Dincă, *J. Am. Chem. Soc.*, 2011, **133**, 20126–20129.
38 Z. Wei, Z.-Y. Gu, R. K. Arvapally, Y.-P. Chen, R. N. McDougald, J. F. Ivy, A. A. Yakovenko, D. Feng, M. A. Omary and H.-C. Zhou, *J. Am. Chem. Soc.*, 2014, **136**, 8269–8276.
39 Z. Hu, G. Huang, W. P. Lustig, F. Wang, H. Wang, S. J. Teat, D. Banerjee, D. Zhang and J. Li, *Chem. Commun.*, 2015, **51**, 3045–3048.
40 J. Feng, L. Zeng, K. Chen, H. Fang, J. Zhang, Z. Chi and C. Y. Su, *Langmuir*, 2016, **32**, 12184–12189.
41 J. Zhang, Q. Yang, Y. Zhu, H. Liu, Z. Chi and C. Y. Su, *Dalton Trans.*, 2014, **43**, 15785–19790.
42 L. Valenzano, B. Civalleri, S. Chavan, S. Bordiga, M. H. Nilsen, S. Jakobsen, K. P. Lillerud and C. Lamberti, *Chem. Mater.*, 2011, **23**, 1700–1718.
43 H. Wu, Y. Chua, V. Krungleviciute, M. Tyagi, P. Chen, T. Yildirim and W. Zhou, *J. Am. Chem. Soc.*, 2013, **135**, 10525–10532.
44 M. J. Katz, Z. J. Brown, Y. J. Colón, P. W. Siu, K. A. Scheidt, R. Q. Snurr, J. T. Hupp and O. K. Farha, *Chem. Commun.*, 2013, **49**, 9449–9451.
45 L. Sarkisov and A. Harrison, *Mol. Simul.*, 2011, **37**, 1248–1257.
46 F. Vermoortele, B. Bueken, G. Le Bars, B. Van de Voorde, M. Vandichel, K. Houthoofd, A. Vimont, M. Daturi, M. Waroquier, V. Van Speybroeck, C. Kirschhock and D. E. De Vos, *J. Am. Chem. Soc.*, 2013, **135**, 11465–11468.
47 G. C. Shearer, S. Chavan, J. Ethiraj, J. G. Vitillo, S. Svelle, U. Olsbye, C. Lamberti, S. Bordiga and K. P. Lillerud, *Chem. Mater.*, 2014, **26**, 4068–4071.
48 W. Liang, C. J. Coghlan, F. Ragon, M. Rubio-Martinez, D. M. D'Alessandro and R. Babarao, *Dalton Trans.*, 2016, **45**, 4496–4500.
49 J. Yang, Z. Wang, K. Hu, Y. Li, J. Feng, J. Shi and J. Gu, *ACS Appl. Mater. Interfaces*, 2015, **7**, 11956–11964.
50 Q.-Y. Li, Z. Ma, W.-Q. Zhang, J.-L. Xu, W. Wei, H. Lu, X. Zhao and X.-J. Wang, *Chem. Commun.*, 2016, **52**, 11284–11287.
51 B. Joarder, A. V. Desai, P. Samanta, S. Mukherjee and S. K. Ghosh, *Chem.–Eur. J.*, 2015, **21**, 965–969.
52 Y. Rachuri, B. Parmar, K. K. Bisht and E. Suresh, *Dalton Trans.*, 2016, **45**, 7881–7892.
53 Z. Hu, B. J. Deibert and J. Li, *Chem. Soc. Rev.*, 2014, **43**, 5815–5840.
54 S. S. Nagarkar, B. Joarder, A. K. Chaudhari, S. Mukherjee and S. K. Ghosh, *Angew. Chem., Int. Ed.*, 2013, **52**, 2881–2885.